Biophysical Journal
Article

Biophysical Society

Investigating the Structure of Multicomponent Gel-Phase Lipid Bilayers

Remco Hartkamp,[1,2] Timothy C. Moore,[1,2] Christopher R. Iacovella,[1,2] Michael A. Thompson,[4] Pallav A. Bulsara,[4] David J. Moore,[4] and Clare McCabe[1,2,3,*]

[1]Department of Chemical and Biomolecular Engineering, [2]Multiscale Modeling and Simulation (MuMS) Center, and [3]Department of Chemistry, Vanderbilt University, Nashville, Tennessee; and [4]GlaxoSmithKline Consumer Healthcare, Warren, New Jersey

ABSTRACT Single- and multicomponent lipid bilayers of 1,2-dipalmitoyl-*sn*-glycero-3-phosphatidylcholine (DPPC), 1,2-distearoyl-*sn*-glycero-3-phosphatidylcholine (DSPC), isostearyl isostearate, and heptadecanoyl heptadecanoate in the gel phase are studied via molecular dynamics simulations. It is shown that the structural properties of multicomponent bilayers can deviate strongly from the structures of their single-component counterparts. Specifically, the lipid mixtures are shown to adopt a compact packing by offsetting the positioning depths at which different lipid species are located in the bilayer. This packing mechanism affects the area per lipid, the bilayer height, and the chain tilt angles and has important consequences for other bilayer properties, such as interfacial hydrogen bonding and bilayer permeability. In particular, the simulations suggest that bilayers containing isostearyl isostearate or heptadecanoyl heptadecanoate are less permeable than pure 1,2-dipalmitoyl-*sn*-glycero-3-phosphatidylcholine or DSPC bilayers. Furthermore, hydrogen-bond analysis shows that the residence times of lipid-water hydrogen bonds depend strongly on the bilayer composition, with longer residence times for bilayers that have a higher DSPC content. The findings illustrate and explain the fundamental differences between the properties of single- and multicomponent bilayers.

INTRODUCTION

Experimental studies have shown that lipid composition can significantly impact membrane properties, e.g., altering in-plane structure, repeat distance, and permeability (1). Determining the molecular mechanisms responsible for these changes is of the utmost importance for rationally designing and engineering lipid mixtures with precisely tuned properties. However, the underlying molecular mechanisms often remain elusive to experimental methods, as behavior must typically be inferred from various experimental measurements, rather than directly measured. As a molecular-level probe, computer simulations provide a means to directly examine lipid structure, dynamics, and thermodynamic properties. Molecular dynamics (MD) simulations in particular have been instrumental in elucidating the molecular arrangement and interactions of lipid membranes (2,3), providing important information with regard to how headgroup structure influences phase behavior, mechanical properties, hydrogen bonding, and transport properties (4–8).

To date, computational studies of lipid membranes have been overwhelmingly focused on phospholipid membranes, such as 1,2-dipalmitoyl-*sn*-glycero-3-phosphatidylcholine (DPPC) (2,9), in large part due to the dominance of phospholipids in biological systems. Furthermore, most of these studies have focused on fluid-phase (i.e., liquid-crystalline) systems, as the slow dynamics of the densely packed lipids in the gel phase require long simulation times and thus incur a high computational cost to reach and sample equilibrium states for atomistically detailed models. Less is therefore known about the structure and properties of gel-phase phospholipid systems, with only a handful of atomistically detailed studies examining the links between composition and structure. Early simulation studies of the gel phase by Tu et al. (10) and Essmann et al. (11) provided some molecular-level interpretation of the available experimental work in terms of the bilayer structure and water-lipid interface. However, noticeable deviation is observed with regard to tail arrangement and headgroup orientation, likely as a consequence of the limited timescales that could be considered (12). Furthermore, the bilayers in these studies showed unphysical conformations as a result of constraining the area per lipid (APL), as was later shown by Venable et al. (13), who found that fluctuations in the simulation-box size are

Submitted May 11, 2016, and accepted for publication July 11, 2016.

*Correspondence: c.mccabe@vanderbilt.edu

Editor: Scott Feller.

http://dx.doi.org/10.1016/j.bpj.2016.07.016

essential during the equilibration stage to form a gel conformation consistent with experiments on a dipalmitoylphosphatidylcholine (DMPC) bilayer. More recent simulations of single-component phospholipid bilayers in the gel phase have revealed that their structure is largely determined by the lipid headgroup size (14,15), a finding supported by experiments showing that the APL does not strongly depend on lipid chain length (16). In comparison, with increasing tail length, fluid-phase membranes show a decrease in APL associated with the stronger van der Waals attraction between the longer tails (17). Other simulation studies have focused on the phase transition from a fluid- to a gel-phase bilayer for DPPC, identifying three distinct structures relative to the transition temperature (18). Of particular interest is the work of Coppock and Kindt (19), who studied a mixture of different-chain-length phospholipids in the gel phase and found an offset in headgroup positions between the different lipid species, with shorter lipids sitting deeper in the bilayer structure. Although increases in computational power have enabled these recent studies to begin probing properties of gel-phase phospholipid systems (14,15), a full understanding of the molecular mechanisms underlying gel-phase lipid systems, and particularly mixed-lipid systems with emollients, has yet to be established.

Here, the behaviors of pure and mixed lipid gel bilayers are examined via MD simulation. Two phospholipid molecules, DPPC and 1,2-distearoyl-*sn*-glycero-3-phosphatidylcholine (DSPC), are considered. DPPC is the phospholipid system most commonly studied via computation, providing validation and a baseline for comparison; DSPC is structurally similar to DPPC, with the same phosphatidylcholine headgroup but longer hydrocarbon tails, as shown in Fig. 1, and is commonly used in the healthcare industry. Two known emollients, isostearyl isostearate (ISIS) and heptadecanoyl heptadecanoate (HDHD), which differ only in their terminal groups (Fig. 1), are also considered. ISIS is of particular interest, as it has been shown experimentally to induce a hexagonal-to-orthorhombic transition in the lateral packing of the hydrocarbon chains of gel-phase ceramide-based bilayer systems (20). This change in structure is suggested to be responsible for the observed reduced permeability (21), although contradictory observations in vivo (17) suggest that the permeability-reducing effect is due to ISIS-induced changes in the lamellar phase behavior of the lipid mixture (22). We also note that studies of side-branched phospholipids have shown that side branches on lipid tails reduce the bilayer permeability by limiting the diffusional freedom of small permeating molecules (23), providing yet another possible mechanism.

Collectively, the lipids studied here enable a comprehensive examination of headgroup size and the effects of chain branching on the structural properties of gel-phase bilayers in pure and mixed lipid systems. The remainder of this article is organized as follows. In Materials and Methods, we discuss the preparation and details of the simulations performed. We then present and discuss our results and, finally, summarize our findings and draw conclusions.

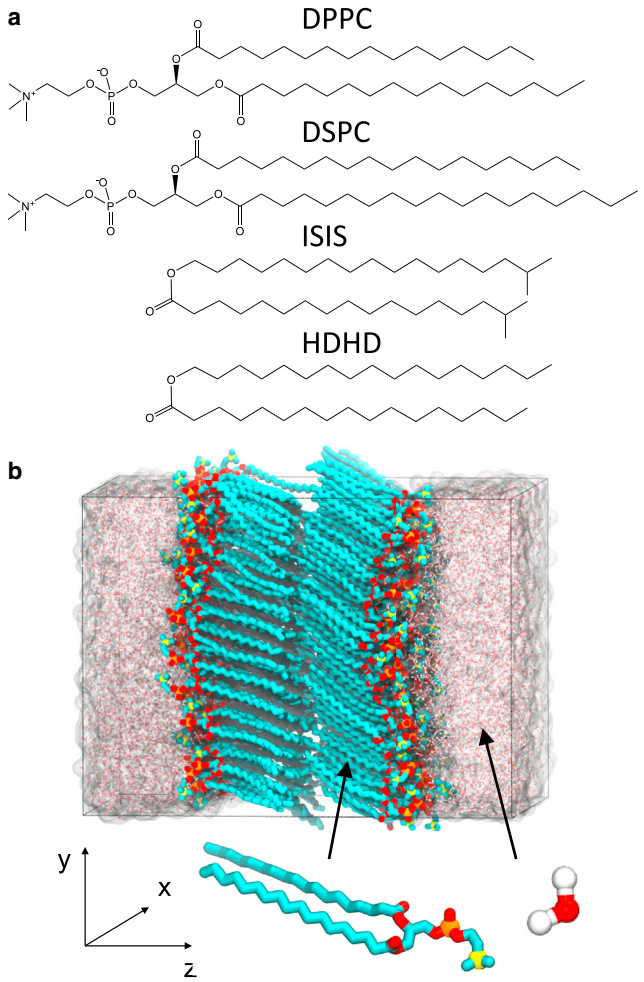

FIGURE 1 (*a*) The structure of the DPPC, DSPC, ISIS, and HDHD lipid molecules examined in this study. (*b*) A snapshot of a typical configuration of a pure DSPC bilayer in water. Hydrocarbons are shown in cyan, oxygen in red, phosphorus in orange, nitrogen in yellow, and hydrogen in white. To see this figure in color, go online.

MATERIALS AND METHODS

A bilayer leaflet was created by placing 100 molecules, in a hairpin configuration, on a square lattice, with tails in the all-*trans* conformation and oriented along the vector perpendicular to the lattice plane. Molecules were randomly rotated along their long axis to create a disordered distribution of lipid backbone orientations, in agreement with the findings of a recent study by Uppulury et al. (24), who showed that disorder in the glycerol orientation is essential for a gel-phase phospholipid bilayer to accurately reproduce the experimentally measured tilt of the lipid tails. The authors suggested that disordered backbone orientations were required, since the reorientation timescale is too long to sample in atomistic simulations. The study presented here uses an initial APL of 56 $Å^2$ to further ensure that the molecules can rearrange and adopt a preferred packing. Furthermore, in the mixed lipid bilayers studied, different molecules

were randomly assigned to lattice sites, mimicking a mixed morphology. A bilayer was then formed by placing two different leaflets parallel to each other, with the tail endings from both leaflets reaching the middle of the bilayer. The bilayers are in excess water to allow for a fair comparison between systems. Each of the bilayers is surrounded by 8000 water molecules (40 per lipid).

The lipids were described by the GROMOS 53a6 force field (25). The partial charges from Chiu et al. (26) were applied to the DPPC and DSPC molecules, whereas the other molecules were created with the Automated Topology Builder, Version 2.1 (27). Water was modeled with the simple-point-charge model, with the rigid structure preserved using the SHAKE algorithm. MD simulations were performed using the LAMMPS simulation engine (28). The simulation box was orthogonal and fully periodic. Dispersion interactions were described by a Lennard-Jones potential, with a cutoff distance of 14 Å. The particle-particle particle-mesh method was used to calculate electrostatic interactions, with the real part truncated at 14 Å (29). The simulation systems were first subjected to an energy minimization, followed by a short run of 100 ps in the NP_zAT ensemble using a time step of 0.5 fs, where the z-direction corresponds to the bilayer normal. The normal pressure was kept at 1 atm and the temperature at 305 K via a Nosé-Hoover thermostat with a coupling time constant of 100 times the simulation time step. The simulations were then switched to the NPT ensemble with anisotropic pressure control and the time step was increased to 2 fs.

Recent studies by Schubert et al. (30) and Uppulury et al. (24) demonstrated that results of gel-phase simulations could depend on the equilibration protocol, which can result from slow dynamics and the presence of ergodic hindrances and various metastable states. Reaching the minimum energy configuration in such systems therefore remains challenging, and although no equilibration procedure ensures this, it is widely recognized that simulated annealing can be instrumental in producing a relaxed configuration (18,31,32). However, it must be noted that simulated cooling rates are typically orders of magnitude higher than the rates commonly used in real annealing. Consequently, the fast annealing used in simulation studies might still not allow sufficient time for a disordered state to become ordered, as suggested by the works of Schubert et al. (30) and Uppulury et al. (24) In an effort to avoid these issues, here, the molecules are initially placed in an already ordered lamellar state with randomized lipid backbone orientations, and a repeated heating and cooling process is performed to increase the lipid lateral movement. Fig. 1 *b* shows a typical simulation snapshot of an equilibrated DSPC bilayer. To validate reproducibility of the results, the equilibrations of multiple DSPC systems are compared and discussed in Fig. S1 in the Supporting Material, and additional details are also provided in the Equilibration Protocol section of the Supporting Material.

All production runs were for 150 ns, of which the last 80 ns was used for analysis. Various structural quantities have been calculated for each system studied to quantify the bilayer properties. These include the APL, which is the cross-sectional area divided by the number of lipids, the acyl chain tilt angle, θ, the bilayer height, and the area per tail (APT), which is the APL divided by the number of tails per molecule and multiplied by $cos(\theta)$ to map the area from the bilayer plane onto the plane perpendicular to the chain directions. The Supporting Material provides detailed information on how each of these quantities was calculated.

RESULTS AND DISCUSSION

Structure of single-component lipid bilayers

To first validate the procedures used in this work, simulations of pure DPPC are performed and compared to the literature. As reported in Table 1, for pure DPPC, an APL of 50.9 (0.2) $Å^2$, APT of 20.7 (0.1) $Å^2$, bilayer height of 44.1 (1.9) Å, and a tilt angle of $\theta = 35.4\ (0.8)^\circ$ were obtained at 305 K. These values are in reasonable agreement with other simulation studies that utilize different force fields. For example, Tjörnhammar and Edholm (15) optimized united-atom force-field parameters for DPPC and found an APL of 47.7 $Å^2$ at 293 K and an average chain tilt angle of $\theta = 31.0\ (1.0)^\circ$, whereas Schubert et al. (30) reported an APL of 50.0 $Å^2$ and an average chain tilt angle of $\theta = 37.0\ (1.0)^\circ$ for DPPC at 300 K, using the united-atom OPLS force field. The simulation results for DPPC also agree with experimental work. For example, for DPPC at 298 K, Sun et al. (16) measured, from x-ray scattering experiments, an APL of 47.3 (0.3) $Å^2$, an APT of 20.2 (0.2) $Å^2$, a bilayer height of 42.8 (0.2) Å, and a chain tilt angle of $\theta = 31.6\ (0.4)^\circ$, whereas other works report APLs of 48.7 Å (2,33) and 52.3 Å (2,34) and a tilt angle of $\theta = 32.6^\circ$ from x-ray diffraction also at 298 K (35). As recently noted by Poger et al., such a range in reported APL values is common (36).

The pure DSPC bilayer simulations produced an APL of 49.7 (0.2) $Å^2$, which is slightly lower than for DPPC, and a tilt angle of $\theta = 36.3\ (0.4)^\circ$, similar to that of DPPC. The lower APL can be explained by the increased van der Waals attraction between the longer acyl chains. Although it is known from experiments that the influence of chain length on APL is smaller in the gel phase than in the liquid-crystalline phase, this has not yet been studied computationally (16,37). The results for the pure DSPC bilayer agree well with values reported in the literature. For example, using x-ray scattering, Sun et al. (16) reported for DSPC at 298 K an APL of 47.3 (0.5) $Å^2$, an APT of 19.8 (0.1) $Å^2$, a bilayer height of 47.0 (0.4) Å, and an average chain tilt angle

TABLE 1 Overview of Structural Properties Determined for Pure and Multicomponent Bilayers

	APL ($Å^2$)	APT ($Å^2$)	H_{PP} (Å)	H_{II} (Å)	H_{HH} (Å)	θ (°)
DPPC	50.9 (0.2)	20.7 (0.1)	44.1 (1.9)			35.4 (0.8)
DSPC	49.7 (0.2)	20.0 (0.1)	48.4 (1.6)			36.3 (0.4)
ISIS	45.5 (0.1)	20.5 (0.1)		40.2 (1.8)		25.5 (0.2)
HDHD	39.5 (0.1)	19.6 (0.1)			43.0 (1.3)	7.6 (1.2)
DSPC-ISIS	42.5 (0.1)	20.1 (0.1)	54.8 (1.7)	41.5 (1.7)		18.8 (0.8)
DSPC-HDHD	40.0 (0.2)	19.7 (0.1)	55.4 (1.3)		43.1 (1.4)	9.4 (1.2)
ISIS-HDHD	40.1 (0.2)	19.8 (0.1)		42.2 (1.6)	45.0 (1.6)	8.4 (0.8)
DSPC-ISIS-HDHD	40.1 (0.2)	19.8 (0.1)	55.8 (1.4)	42.2 (1.4)	44.3 (1.4)	8.9 (2.2)

The numbers in parentheses are error estimates based on the standard deviation.

of $\theta = 32.5\ (0.4)^\circ$. Tardieu et al. (38) performed x-ray scattering experiments at 293 K and found a larger APL of 52.0 $Å^2$ and an average chain tilt angle of $\theta = 38^\circ$. An even larger APL of 54.7 $Å^2$ was found by Lis et al. (34) using x-ray diffraction at 298 K. Using molecular simulations, Coppock and Kindt (19) obtained an APL of 50.2 $Å^2$ and an average chain tilt angle of $\theta = 37.5^\circ$ for DSPC at 313 K using the united-atom force field of Berger (39). The data reported here are in good agreement with these earlier results and serve to further validate our simulation findings.

The pure ISIS bilayer to our knowledge has not been previously studied. The APL of the ISIS bilayer, as reported in Table 1, is found to be 45.5 (0.1) $Å^2$, which is smaller than the values of 50.9 (0.2) $Å^2$ and 49.7 (0.2) $Å^2$ obtained for DPPC and DSPC, respectively, owing to the small ester headgroup. Similarly, the tilt angle of 25.5 (0.5)° determined for ISIS is smaller than the values of 35.4 (0.8)° and 36.3 (0.4)° found for DPPC and DSPC, respectively. However, the tilt angle of the ISIS tails is still large, which indicates that the APL remains considerably larger than would be desirable based on the tail-tail interactions alone. This behavior can have one of two causes: 1) it could be related to the size of the headgroups and the presence of water molecules between them, or 2) it may be a consequence of the steric repulsions between the side branches on the acyl chains. The latter possibility can be tested by comparing the structural properties of the ISIS and HDHD bilayers. The data in Table 1 report that the HDHD bilayer has an APL of 39.5 (0.1) $Å^2$ and a tilt angle of 7.6 (1.2)°, both of which are considerably smaller than the values found for the ISIS bilayer. These data show that the small ester headgroup is not prohibitive in the formation of a densely packed gel bilayer, indicating that the methyl side branches in ISIS are responsible for the large APL and tilt angle observed. As such, the results illustrate that although the APL and tilt angle of the single-component gel-phase bilayers do not strongly depend on tail length, they do depend on the headgroup chemistry and branching (i.e., cross-sectional area) of the tails.

Equimolar lipid mixtures

The DSPC-ISIS mixture is considered first and reported in Table 1. This mixture is found to have a much smaller APL than either the pure DSPC or pure ISIS bilayers, resulting in a smaller tilt angle and a larger bilayer height. Although it is counterintuitive that the APL of the mixture is smaller than that of either single-component bilayer, this can be partially explained by the fact that only half of the molecules in the DSPC-ISIS bilayer contain a large headgroup and only half of the tails contain side branches. This reduces the steric repulsions between these large groups and thus allows for a smaller APL. The APT of the DSPC-ISIS bilayer shows no significant deviation from that of the pure DSPC and ISIS bilayers, but the fact that the value is slightly higher than that of the pure HDHD bilayer indicates that the presence of the large head and tail groups still prevents a denser chain packing. The mass-density profile of the heads and tails of the DSPC-ISIS bilayer, shown in Fig. 2, reveals an important feature in the structure of this mixture; the headgroups and the tails of the different types of molecules are located at different depths in the bilayer, with ISIS located deeper in the bilayer. A small difference between headgroup depths of different molecules was also observed by Coppock and Kindt, who simulated a gel-phase DSPC-DMPC mixture and found that the heads of the DMPC molecules were located 0.1–0.2 nm deeper in the bilayer than the DSPC heads (19). The spatial arrangement of the molecules in the DSPC-ISIS mixture is shown in Fig. 3, *c* and *e*. The offset in depth can be quantified for the headgroups as $\Delta = (H_{PP} - H_{II})/2 = 6.4$ Å, which defines the distance between the average depth of the phosphate group and the ISIS headgroup in a bilayer, where H_{PP} and H_{II} are the bilayer heights based on the phosphate and ISIS headgroups, respectively. As a consequence of the offset, the large DSPC headgroups, which are now only present on half of the molecules, are not hindered much by ISIS headgroups. Similarly, the ISIS tail endings are located near the middle of the bilayer, where the bilayer density is reduced. Thus,

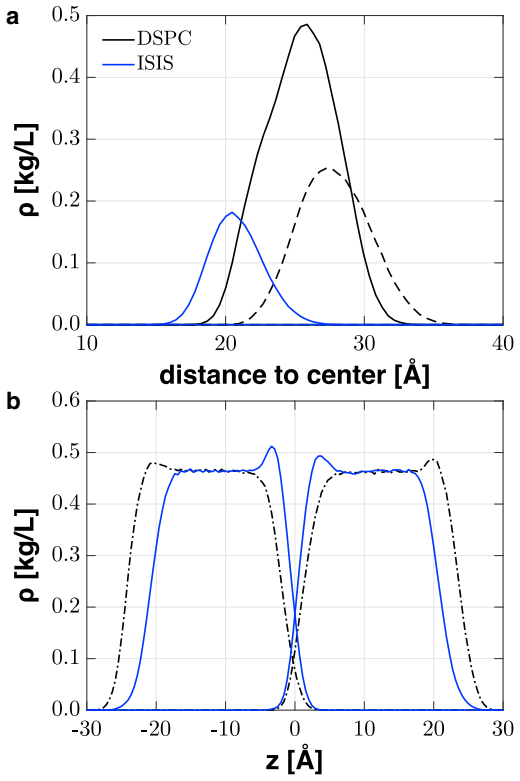

FIGURE 2 (*a*) Headgroup and (*b*) tail mass density profiles of a DSPC-ISIS bilayer. The DSPC headgroup density is decomposed into the choline density (*dashed black line*) and the phosphate/glycerol density (*solid black line*). To see this figure in color, go online.

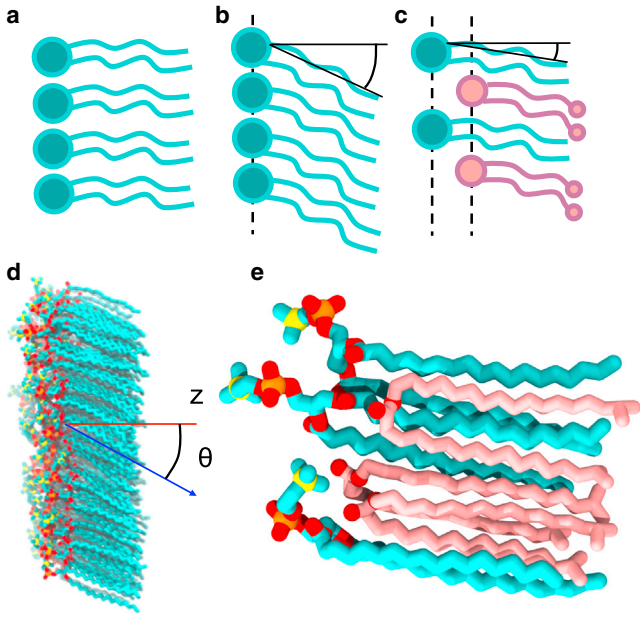

FIGURE 3 Illustration of the lipid packing. (*a*) When large headgroups are packed together, the distance between lipid tails can be larger than is energetically preferable. (*b*) Chain tilt with respect to the bilayer normal decreases the distances between the chains. (*c*) A more compact packing is possible, without the need for large tilt, when two lipid types have their heads located at different depths. (*d*) A simulation snapshot of a leaflet, showing the orientation of the tilted chains (*blue arrow*). (*e*) A simulation snapshot showing how DSPC and ISIS are positioned relative to each other. To see this figure in color, go online.

a compact packing of the molecules is achieved by mitigating the large steric repulsions between headgroups and tail endings. This results in an APL and a chain tilt angle that are much smaller than in the single-component bilayers. The more compact packing reduces the cross-sectional area of the bilayer, whereas the offset increases the effective interfacial area, allowing more water molecules to hydrate the protruding DSPC headgroups. This naturally has consequences for hydrogen-bonding interactions as well as bilayer permeability, as discussed below.

Although the offset can be explained by the need to mitigate repulsions between headgroups and tails, the DSPC-ISIS results alone do not reveal which parts of the molecules represent the driving force behind the offset. However, this can be determined by also investigating the structure of DSPC-HDHD and ISIS-HDHD bilayers, which eliminate the presence of side branches and large headgroups, respectively. The data in Table 1 suggest that the structure of the DSPC-HDHD bilayer deviates from that of the DSPC-ISIS bilayer, consistent with the differences between the pure ISIS and HDHD bilayers. That is, the APL, APT, and tilt angle of DSPC-HDHD are very similar to those of pure HDHD, indicating that the large size of the DSPC headgroups does not determine the packing density of the lipids in an equimolar mixture. The offset between the headgroup positions is $\Delta = (H_{PP} - H_{HH})/2 = 6.2$ Å, where H_{HH} is the average distance between the HDHD headgroups in both leaflets of the bilayer and is only slightly smaller than for DSPC-ISIS. Note however, that even if the offset were the same as for DSPC-ISIS, the distances between the headgroups would be smaller for DSPC-HDHD due to the smaller APL. The fact that the offset is reduced, despite a smaller APL, demonstrates that headgroup repulsions are not responsible for the large offset in the DSPC-ISIS bilayer, showing that the side branches cause the large offset, which can be corroborated by data for the ISIS-HDHD bilayer. The APL, APT, and tilt angle of the ISIS-HDHD bilayer are again similar to those of pure HDHD, with the side branches on the ISIS molecules causing a slight increase in these measures. Although ISIS and HDHD have the same headgroups and tail lengths, the equimolar mixture of these lipids shows an offset of 1.4 Å between the headgroup positions. The ISIS molecules are again positioned deeper into the bilayer, such that the tail endings escape the dense tail area in the middle of the bilayer. This offset is clearly driven solely by the side branches on the ISIS tails, since the headgroup and tail length of ISIS and HDHD are identical.

The results presented so far have elucidated how the molecular geometries determine the bilayer structure of binary mixtures through a balance between steric repulsions and van der Waals attractions. An equimolar DSPC-ISIS-HDHD bilayer has also been studied to determine whether the insights from the binary mixtures extend to more complex systems. The data presented in Table 1 show that the structural properties of the three-component mixture are very similar to those of the other bilayers containing HDHD. These systems are all characterized by small APL, APT, and tilt angle, compared to the bilayers without HDHD. The three-component bilayer shows an extended offset mechanism, in which the ISIS molecules are located deepest in the bilayer, the DSPC molecules are found furthest toward the exterior, and the HDHD molecules are in an intermediate position. The role of the HDHD lipids can be seen as that of a "filler molecule," allowing sufficient space for the lipids that contain larger groups. Based on the findings presented, we believe that adding small amounts of HDHD to a DSPC or ISIS bilayer would strongly affect the bilayer structure until the steric repulsions are sufficiently reduced, after which adding more HDHD will have a minimal effect.

Water-lipid hydrogen-bonding analysis

Hydrogen bonding affects bilayer structure, lipid dynamics, and the dynamics of fluid molecules in the bilayer headgroup region (40). Since the lipids in this study have no explicit (polar) hydrogen atoms, they can only form hydrogen bonds with nearby water molecules, not with other lipids. The calculated average numbers of hydrogen bonds between a DPPC, DSPC, ISIS, or HDHD molecule and the surrounding water molecules are presented in Table 2

TABLE 2 Average Number of Lipid-Water Hydrogen Bonds per Lipid Molecule in Each of the Bilayers Studied

	DSPC					
	Total	Phos.	Glyc.	Tails	ISIS	HDHD
DPPC	3.42 (0.12)	0.652	0.022	0.326		
DSPC	3.29 (0.09)	0.632	0.034	0.334		
ISIS					0.75 (0.06)	
HDHD						0.71 (0.06)
DSPC-ISIS	3.90 (0.14)	0.599	0.041	0.361	0.61 (0.06)	
DSPC-HDHD	3.96 (0.22)	0.619	0.031	0.350		0.55 (0.08)
ISIS-HDHD					0.68 (0.09)	0.80 (0.09)
DSPC-ISIS-HDHD	4.28 (0.24)	0.605	0.036	0.359	0.59 (0.10)	0.58 (0.10)

The average numbers of hydrogen bonds per DPPC and DSPC molecule are decomposed into fractions associated with different parts of the molecule, as shown in Fig. 4. In the ISIS and HDHD molecules, only the headgroups are involved in hydrogen bonds. The numbers in parentheses are error estimates based on the standard deviation.

for all the systems studied. The criterion used to determine the presence of a hydrogen bond was based on a combination of the O···H distance, r_{OH}, being <2.35 Å and the $O_j - O_i \cdots H_i$ angle, $\angle_{OOH}$, being $<30^\circ$, where molecule i is the donor molecule and j the acceptor (41).

The lipids in the pure DPPC and DSPC bilayers form on average 3.4 and 3.3 hydrogen bonds, respectively, with surrounding water molecules. This agrees well with the study by Stępniewski et al. (42), who found a value of 3.61 for DSPC in the gel phase. In comparison, values around 6–7 are typically found in the liquid-crystalline phase, in which more space is available to hydrate the headgroups (42–44). Roughly two-thirds of the hydrogen bonds are found to involve the phosphate group (shown in Fig. 4) and one-third the carbonyl group on either of the lipid tails, which are located deeper in the bilayer. Both groups contain accessible double-bonded oxygen atoms, in contrast to the glycerol backbone of the molecules, which only contains ether oxygens and accounts for only 3% of the hydrogen bonds. The choline headgroup is not listed in Table 2, since this group is found not to form hydrogen bonds. Although the choline headgroup is fully exposed to the aqueous phase, the methyl groups limit the accessibility of the nitrogen atom, in agreement with earlier work. For example, Lopez et al. (40) found for a liquid-crystalline DMPC bilayer that most lipid-water hydrogen bonds were formed at the carbonyl groups and the double-bonded oxygen atoms of the phosphate groups, and that these bonds were longer lived than bonds formed with other acceptor atoms. Similarly, Leekumjorn and Sum (43) determined that for liquid-crystalline DPPC, 58% of the water-lipid hydrogen bonds involved the phosphate group and 34% the carbonyl groups on the lipid tails, in close agreement with the values reported in Table 2. Furthermore, consistent with the observation made here, neither study found hydrogen bonds between water and the nitrogen atom in the choline group.

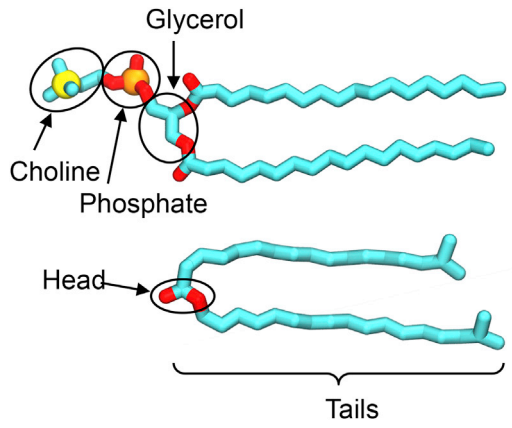

FIGURE 4 The hydrogen-bonding groups within the phospholipids (*top*) and emollients (*bottom*). The circled groups are considered headgroups, whereas the remaining parts of the molecules are the tails. To see this figure in color, go online.

A comparison between the pure bilayers shows that DPPC and DSPC form more hydrogen bonds than ISIS and HDHD. This is not surprising, since the phospholipids contain more potential hydrogen-bond acceptor atoms and their headgroups are much more hydrated than the ester headgroups of ISIS and HDHD. ISIS and HDHD have identical headgroups, and the larger number of hydrogen bonds seen for the ISIS compared to the HDHD bilayer is consistent with its larger APL.

Mixtures involving DSPC exhibit more hydrogen bonds per DSPC molecule compared to the pure DSPC bilayer. As the mole fraction of DSPC decreases, the accessibility of protruding DSPC headgroups increases. This applies to each of the hydrogen-bond acceptors in the DSPC molecule, because the ISIS and HDHD headgroups are located as deep in the bilayer as the carbonyl groups of the DSPC molecules. As a result, the proportions to which the different parts of the DSPC molecules contribute to the formation of hydrogen bonds are independent of the bilayer composition. The fact that the ISIS and HDHD headgroups are located deeper in the bilayer interior than the DSPC headgroups causes them to form fewer hydrogen bonds in bilayers that contain DSPC than in bilayers without DSPC. In the latter case, water molecules can partially surround the ester headgroups; which is not possible in the case where ISIS or HDHD molecules are sandwiched between longer

molecules. Even in the ISIS-HDHD mixture, the offset affects hydrogen-bonding numbers, as evidenced by the fact that the ISIS molecules form fewer hydrogen bonds than HDHD due to their deeper position in the bilayer. This offset simultaneously increases the water-accessible space around an HDHD headgroup and decreases the space around an ISIS headgroup.

Table 3 presents, for each bilayer studied, the average residence times of hydrogen bonds between water and the lipid species present in the bilayer. Average residence times are found to depend more strongly on the bilayer composition than on which lipid species is involved in the hydrogen-bond interaction. The dependence on bilayer composition is shown by a decrease in the residence times as the concentration of DSPC decreases, which has two causes. First, a decrease in the number of DSPC headgroups leads to a decrease in the number of double-bonded oxygen atoms that are prone to strong hydrogen bonding. Second, a lower density of DSPC headgroups results in more freedom for water molecules to move around the headgroups, and this increased mobility in turn reduces the residence times. Furthermore, the data show that the average residence times of the hydrogen bonds are approximately similar for each lipid species in the bilayer. This can be explained by the fact that hydrogen-bond residence times depend on the freedom of water molecules to move around and reorient, which depends not only on which lipid the water molecules are hydrogen-bonded to, but also on their local environment (i.e., the bilayer composition).

Water partitioning

The excess-free-energy profile, $\Delta G(z)$, describes the amount of work needed to displace water from the bulk phase to a certain depth in the bilayer. This profile can be calculated from the water-density profile, $\rho(z)$, via a potential of mean force expression:

$$\Delta G(z) = -k_B T \ln(\rho(z)/\rho_0), \quad (1)$$

where $k_B T$ is the thermal energy, ρ_0 denotes the bulk water density far from the bilayer, and the ratio between the two densities, $n(z) = \rho(z)/\rho_0$, is the density of states. Fig. 5 presents the excess-free-energy profiles for a subset of the systems studied, for the sake of clarity, whereas the data for the other systems are shown in Fig. S2. The profiles are displayed as the distance from the bilayer center, which means that the profiles are horizontally separated due to the different bilayer heights. The data show that the bilayers containing ISIS or HDHD have a steep slope in the energy profiles toward the dense tail region, whereas the profiles corresponding to pure DPPC and DSPC bilayers have a much smaller slope, indicating that a water molecule can reach the interior of the DPPC and DSPC bilayers at a smaller free-energy cost. The steep energy slopes obtained for bilayers containing ISIS supports the claim that ISIS reduces the permeability of a bilayer (20). In addition, the data suggest that the presence of HDHD in a bilayer also reduces bilayer permeability, based on this measure.

Once a water molecule reaches the bilayer interior, the speed at which it diffuses through the bilayer depends on the available space, which varies across the bilayer. The available space at a given depth is complementary to the amount of space occupied by the lipids, which can be calculated by defining a plane perpendicular to the transmembrane axis and measuring the fraction of the plane area that coincides with the presence of intersected atoms (45). Occupied-area profiles are especially valuable for bilayers in the gel phase, since the dense chain packing does not allow for large thermal fluctuations in space between lipid tails ("pockets"), and the regular lipid packing leads to small variations between pocket sizes. Since all the pockets are approximately the same size, the average occupied area is representative of the local environment in the bilayer. Thus, the diffusional freedom in the different gel-phase bilayers can be compared qualitatively by comparing their occupied-area profiles. The details of this calculation are provided in the Supporting Material.

The occupied-area profiles for all the systems studied are presented in Fig. 6. The maximum occupied-area fraction

TABLE 3 Residence Times of Hydrogen Bonds between a Water Molecule and a Lipid Species in Each of the Bilayer Systems Studied

	DSPC	ISIS	HDHD
DPPC	192.3		
DSPC	194.1		
ISIS		27.3	
HDHD			27.4
DSPC-ISIS	66.6	58.4	
DSPC-HDHD	84.2		78.0
ISIS-HDHD		29.5	27.3
DSPC-ISIS-HDHD	56.3	49.7	42.8

All times are given in picoseconds.

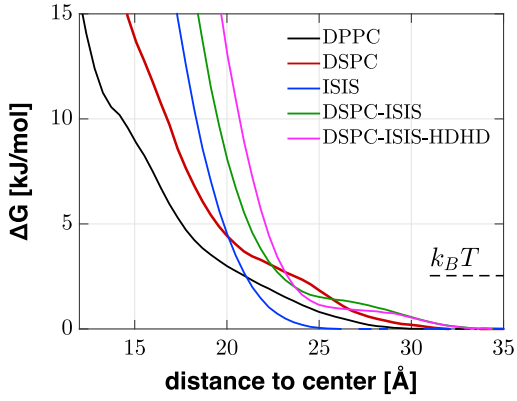

FIGURE 5 The excess-free-energy profiles for water molecules to penetrate into bilayers. To see this figure in color, go online.

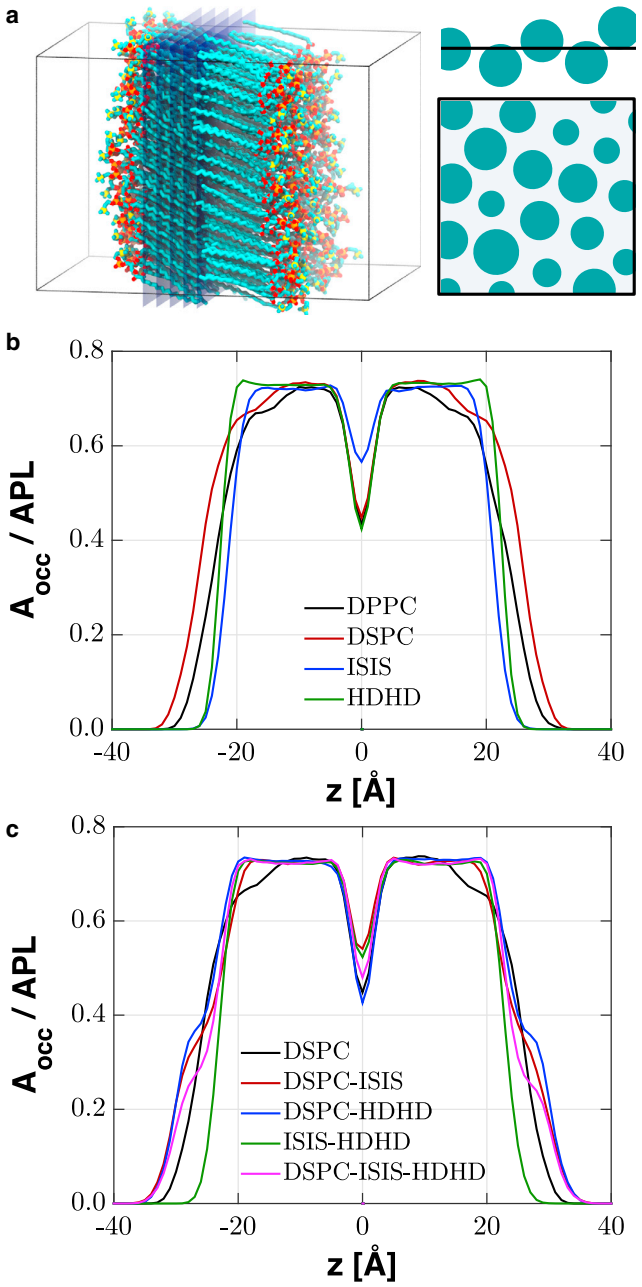

FIGURE 6 The fraction of occupied area across a bilayer. (*a*) Left: Planes intersect the bilayer at various positions along the bilayer normal. Right: A representation of the side (*top*) and front (*bottom*) views of an intersecting plane. The side view shows that some atoms are intersected through the middle; these contribute a larger occupied area on the plane than atoms that are intersected very close to the edge. (*b*) Occupied-area profiles corresponding to single-component bilayers. (*c*) Occupied-area profiles corresponding to mixed-lipid bilayers, with the pure DSPC bilayer profile as a reference. To see this figure in color, go online.

for each of the bilayers is ~0.72–0.74, which is notably larger than the 0.65 measured for DPPC in the liquid-crystalline phase (46). DPPC and DSPC show narrow dense regions compared to the other profiles, which all show a dense plateau in the tail region. The fact that DSPC is locally very dense might seem surprising given the large APT of the bilayer; however, the occupied-area profiles of DPPC and DSPC both suggest that the density in the tail region varies along the length of the chains, such that the reported APT is an effective average value. This variation along the chain length can be explained by the van der Waals attraction between the chains. It is not possible for the chains to be closer to each other near the headgroup region, whereas there are no obstacles farther from the headgroups. This results in the DSPC tails being slightly curved, so that the tail-tail distances are smaller toward the middle of the bilayer, and thus, the occupied area and the tilt angle are larger in this region. The occupied-area profiles corresponding to the pure ISIS and HDHD bilayers show a dense plateau value in the tail region and a slightly increased density in the headgroup region, especially for HDHD, due to its smaller APL. This large occupied area can form a significant barrier to water molecules entering the bilayer and is thus indicative of a small bilayer permeability, as was also suggested by the excess-free-energy profiles discussed earlier in this section.

All of the mixed-lipid systems studied show a dense plateau region similar in shape to that of the pure ISIS and HDHD bilayers. However, the plateaus are wider for the mixtures, due to the small tilt angles and the offsets observed in these bilayers. Combining the wide, dense plateaus with the large free energy of partitioning of the mixed bilayers that contain ISIS or HDHD, it appears that these bilayers are less permeable than the pure DPPC and DSPC bilayers. The occupied area in the bilayer center depends strongly on the amount of ISIS present in the system, since the tail endings of ISIS molecules are bulky and located closer to the bilayer center than the other tail endings, to mitigate steric repulsions between these side-branched tails. Consequently, the occupied areas in the bilayer center of systems that are rich in ISIS are more similar to the dense tail region. The increased presence of methyl groups in the bilayer center could reduce the residence time for water molecules in the middle of the bilayer, since the relatively dense and hydrophobic center is not strongly preferable environment for water molecules over the dense hydrophobic tail region. However, the side branches of the ISIS molecules could also form an obstacle for water molecules to pass (23).

Bilayer permeability is typically calculated using the inhomogeneous solubility-diffusion model, in which the permeability coefficient is calculated from a one-dimensional integral function containing the excess-free-energy and diffusion-coefficient profiles (46). The computations needed to calculate these profiles are computationally expensive, particularly for a gel-phase bilayer due to the slow dynamics. When one is interested in finding how various lipid components and compositions affect the bilayer permeability, it is thus not practical to calculate the permeability for a large number of systems. It is therefore desirable to be able to predict how bilayer compositions

affect the permeability, based on the data available from equilibrium MD simulations. From the inhomogeneous solubility-diffusion model, it is known that the permeability is related to 1) the free-energy cost of displacing a permeating molecule from the aqueous phase to the bilayer interior, and 2) the diffusional freedom of this molecule in the dense tail region, both of which are less computationally expensive calculations than the permeability.

The excess-free-energy and occupied-area profiles calculated support the observations from experimental studies (17,21,22) that ISIS reduces the bilayer permeability and suggest that HDHD has a similar effect on the bilayer permeability. However, it must be noted that these calculated quantities provide limited insight into permeability. For example, the fact that DSPC headgroups are more hydrated in mixed-component bilayers implies that the hydrophobic regions of these bilayers are more exposed to water than in the pure DSPC bilayer. This could result in increasing permeability as the DSPC concentration decreases. A wide, dense tail region and densely packed small headgroups, features that are believed to result in a small bilayer permeability, distinguish the systems with ISIS and HDHD from those dominated by DSPC. Although it is possible that side branches further reduce bilayer permeability, the findings here indicate that they are not the only mechanism responsible for a reduced permeability in the case of ISIS. We note that experimental studies have reported contradictory links between orthorhombic lipid packing and bilayer permeability (17,21,47) and that orthorhombic chain packing was investigated in this study, although the uncertainty in the lattice parameters was found to be larger than the hexagonal-to-orthorhombic deformation, so that no conclusion could be drawn. The chain packing and hexagonal-to-orthorhombic deformation are discussed in Fig. S3.

CONCLUSIONS

The work presented here highlights important new insights, to our knowledge, into the structural properties of single- and multicomponent bilayers in the gel phase. Single-component DPPC, DSPC, and ISIS bilayers showed large APLs and tail tilt, in contrast to those of an HDHD bilayer. It was found that the structures of single-component bilayers depend on the sizes of the different parts of the lipids. In the case of DPPC and DSPC, the large APL was a consequence of the headgroup size, whereas in the case of ISIS molecules, the side branches on the tails prevented a tighter lipid packing. When the lipid molecules contain no bulky parts, such as in the case of HDHD, the APL is largely determined by the interactions between the acyl chains.

The structural properties of lipid mixtures are found to be not simply a combination of the properties of their single-component constituents. In particular, the APL and chain tilt angle of a DSPC-ISIS bilayer are smaller than those of pure DSPC and ISIS bilayers. This is explained first by the fact that only half of the molecules have a large headgroup and only half of the tails have side branches, such that the steric repulsions are much smaller than in single-component bilayers. Second, an offset is formed between the positioning depths of the lipid species in the bilayers, especially when ISIS is present in the bilayer. The side branches on the ISIS tails drive these molecules to be located deeper in the bilayer than other components, enabling the ISIS tail endings to be located outside of the dense tail region. The absence of side branches (i.e., in a DSPC-HDHD bilayer) results in a smaller offset and APL. The fact that the APL decreases despite the decreasing offset demonstrates that headgroup repulsions have less influence on the structure of a multicomponent bilayer than do side branches for the systems studied. The complicated structural arrangements observed for the two- and three-component mixtures illustrate that although the study of single-component model bilayers is important, the properties of multicomponent bilayers can be dominated by mechanisms unique to the molecular interactions present in multicomponent systems.

Hydrogen bonding between water and lipids was investigated, and the number of hydrogen bonds per molecule was found to depend on the bilayer composition. This was especially clear in the case of bilayers containing DSPC: a lower concentration of DSPC resulted in more space around the DSPC headgroups and thus a larger number of hydrogen bonds per DSPC molecule. On the other hand, the residence times of hydrogen bonds decreased with decreasing DSPC concentration, since residence times depend on the local water mobility: More available space around the DSPC headgroups results in more freedom for the water to move around. It was found that the hydrogen-bond residence times for each lipid species in a bilayer were approximate, since the movement of a water molecule depends not only on the lipid that it is hydrogen-bonded to, but also on its local environment, including the surrounding lipids and the spatial confinement.

Finally, bilayer permeability was discussed in terms of the free-energy cost for water to penetrate into the bilayer and the available space to diffuse through the bilayer interior. It was found that ISIS and HDHD result in a steeper free-energy profile compared to DPPC and DSPC, and that the dense tail region is wider in the systems with ISIS or HDHD, compared to the pure DPPC and DSPC bilayers. These results are indicative of a smaller permeability when either of these esters is present in the bilayer.

SUPPORTING MATERIAL

Supporting Materials and Methods, three figures, and one table are available at http://www.biophysj.org/biophysj/supplemental/S0006-3495(16)30579-3.

AUTHOR CONTRIBUTIONS

D.J.M. and C.M. designed research; R.H. performed research; R.H. and T.C.M. contributed analytic tools; all authors analyzed data; and all authors wrote the article.

ACKNOWLEDGMENT

Computational resources were provided by the National Energy Research Scientific Computing Center, supported by the Office of Science of the Department of Energy under contract no. DE-AC02-05CH11231.

REFERENCES

1. Gennis, R. B. 1989. Biomembranes: Molecular Structure and Function. Springer, New York, pp. 36–84.
2. Lyubartsev, A. P., and A. L. Rabinovich. 2011. Recent development in computer simulations of lipid bilayers. *Soft Matter.* 7:25–39.
3. Pluhackova, K., and R. A. Böckmann. 2015. Biomembranes in atomistic and coarse-grained simulations. *J. Phys. Condens. Matter.* 27:323103.
4. Guo, S., T. C. Moore, …, C. McCabe. 2013. Simulation study of the structure and phase behavior of ceramide bilayers and the role of lipid head group chemistry. *J. Chem. Theory Comput.* 9:5116–5126.
5. Vernier, P. T., M. J. Ziegler, and R. Dimova. 2009. Calcium binding and head group dipole angle in phosphatidylserine-phosphatidylcholine bilayers. *Langmuir.* 25:1020–1027.
6. Pasenkiewicz-Gierula, M., Y. Takaoka, …, A. Kusumi. 1997. Hydrogen bonding of water to phosphatidylcholine in the membrane as studied by a molecular dynamics simulation: location, geometry, and lipid-lipid bridging via hydrogen-bonded water. *J. Phys. Chem. A.* 101:3677–3691.
7. Moore, P. B., C. F. Lopez, and M. L. Klein. 2001. Dynamical properties of a hydrated lipid bilayer from a multinanosecond molecular dynamics simulation. *Biophys. J.* 81:2484–2494.
8. Cascales, J. J. L., S. D. O. Costa, …, R. D. Enriz. 2012. Mechanical properties of binary DPPC/DPPS bilayers. *RSC Adv.* 11743–11750.
9. Tieleman, D. P., S.-J. Marrink, and H. J. C. Berendsen. 1997. A computer perspective of membranes: molecular dynamics studies of lipid bilayer systems. *Biochim. Biophys. Acta.* 1331:235–270.
10. Tu, K., D. J. Tobias, …, M. L. Klein. 1996. Molecular dynamics investigation of the structure of a fully hydrated gel-phase dipalmitoylphosphatidylcholine bilayer. *Biophys. J.* 70:595–608.
11. Essmann, U., L. Perera, and M. L. Berkowitz. 1995. The origin of the hydration interaction of lipid bilayers from MD simulation of dipalmitoylphosphatidylcholine membranes in gel and liquid crystalline phases. *Langmuir.* 11:4519–4531.
12. Tobias, D. J., K. Tu, and M. L. Klein. 1997. Atomic-scale molecular dynamics simulations of lipid membranes. *Curr. Opin. Colloid Interface Sci.* 2:15–26.
13. Venable, R. M., B. R. Brooks, and R. W. Pastor. 2000. Molecular dynamics simulations of gel (L-β I) phase lipid bilayers in constant pressure and constant surface area ensembles. *J. Chem. Phys.* 112:4822–4832.
14. Debnath, A., F. M. Thakkar, …, K. G. Ayappa. 2014. Laterally structured ripple and square phases with one and two dimensional thickness modulations in a model bilayer system. *Soft Matter.* 10:7630–7637.
15. Tjörnhammar, R., and O. Edholm. 2014. Reparameterized united atom model for molecular dynamics simulations of gel and fluid phosphatidylcholine bilayers. *J. Chem. Theory Comput.* 10:5706–5715.
16. Sun, W. J., S. Tristram-Nagle, …, J. F. Nagle. 1996. Structure of gel phase saturated lecithin bilayers: temperature and chain length dependence. *Biophys. J.* 71:885–891.
17. Caussin, J., G. S. Gooris, …, J. A. Bouwstra. 2007. Interaction of lipophilic moisturizers on stratum corneum lipid domains in vitro and in vivo. *Skin Pharmacol. Physiol.* 20:175–186.
18. Leekumjorn, S., and A. K. Sum. 2007. Molecular studies of the gel to liquid-crystalline phase transition for fully hydrated DPPC and DPPE bilayers. *Biochim. Biophys. Acta.* 1768:354–365.
19. Coppock, P. S., and J. T. Kindt. 2009. Atomistic simulations of mixed-lipid bilayers in gel and fluid phases. *Langmuir.* 25:352–359.
20. Caussin, J., G. S. Gooris, and J. A. Bouwstra. 2008. FTIR studies show lipophilic moisturizers to interact with stratum corneum lipids, rendering the more densely packed. *Biochim. Biophys. Acta.* 1778:1517–1524.
21. Pilgram, G. S. K., D. C. Vissers, …, H. K. Koerten. 2001. Aberrant lipid organization in stratum corneum of patients with atopic dermatitis and lamellar ichthyosis. *J. Invest. Dermatol.* 117:710–717.
22. Pennick, G., S. Harrison, …, A. V. Rawlings. 2010. Superior effect of isostearyl isostearate on improvement in stratum corneum water permeability barrier function as examined by the plastic occlusion stress test. *Int. J. Cosmet. Sci.* 32:304–312.
23. Tristram-Nagle, S., D. J. Kim, …, J. F. Nagle. 2010. Structure and water permeability of fully hydrated diphytanoylPC. *Chem. Phys. Lipids.* 163:630–637.
24. Uppulury, K., P. S. Coppock, and J. T. Kindt. 2015. Molecular simulation of the DPPE lipid bilayer gel phase: coupling between molecular packing order and tail tilt angle. *J. Phys. Chem. B.* 119:8725–8733.
25. Oostenbrink, C., A. Villa, …, W. F. van Gunsteren. 2004. A biomolecular force field based on the free enthalpy of hydration and solvation: the GROMOS force-field parameter sets 53A5 and 53A6. *J. Comput. Chem.* 25:1656–1676.
26. Chiu, S. W., M. Clark, …, E. Jakobsson. 1995. Incorporation of surface tension into molecular dynamics simulation of an interface: a fluid phase lipid bilayer membrane. *Biophys. J.* 69:1230–1245.
27. Malde, A. K., L. Zuo, …, A. E. Mark. 2011. An automated force field topology builder (ATB) and repository: Version 1.0. *J. Chem. Theory Comput.* 7:4026–4037.
28. Plimpton, S. 1995. Fast parallel algorithms for short-range molecular dynamics. *J. Comput. Phys.* 117:1–19.
29. Hockney, R. W., and J. W. Eastwood. 1988. Computer Simulation Using Particles. Taylor & Francis, Milton Park, United Kingdom.
30. Schubert, T., E. Schneck, and M. Tanaka. 2011. First order melting transitions of highly ordered dipalmitoyl phosphatidylcholine gel phase membranes in molecular dynamics simulations with atomistic detail. *J. Chem. Phys.* 135:055105.
31. Höltje, M., T. Förster, …, H. D. Höltje. 2001. Molecular dynamics simulations of stratum corneum lipid models: fatty acids and cholesterol. *Biochim. Biophys. Acta.* 1511:156–167.
32. Pimthon, J., R. Willumeit, …, D. Hofmann. 2009. All-atom molecular dynamics simulation studies of fully hydrated gel phase DPPG and DPPE bilayers. *J. Mol. Struct.* 921:38–50.
33. Rand, R. P., and V. A. Parsegian. 1989. Hydration forces between phospholipid bilayers. *Biochim. Biophys. Acta.* 988:351–376.
34. Lis, L. J., M. McAlister, …, V. A. Parsegian. 1982. Interactions between neutral phospholipid bilayer membranes. *Biophys. J.* 37:657–665.
35. Katsaras, J., D. S. Yang, and R. M. Epand. 1992. Fatty-acid chain tilt angles and directions in dipalmitoyl phosphatidylcholine bilayers. *Biophys. J.* 63:1170–1175.
36. Poger, D., B. Caron, and A. E. Mark. 2016. Validating lipid force fields against experimental data: progress, challenges and perspectives. *Biochim. Biophys. Acta.* 1858:1556–1565.
37. Petrache, H. I., S. W. Dodd, and M. F. Brown. 2000. Area per lipid and acyl length distributions in fluid phosphatidylcholines determined by ^{2}H NMR spectroscopy. *Biophys. J.* 79:3172–3192.
38. Tardieu, A., V. Luzzati, and F. C. Reman. 1973. Structure and polymorphism of the hydrocarbon chains of lipids: a study of lecithin-water phases. *J. Mol. Biol.* 75:711–733.

39. Berger, O., O. Edholm, and F. Jähnig. 1997. Molecular dynamics simulations of a fluid bilayer of dipalmitoylphosphatidylcholine at full hydration, constant pressure, and constant temperature. *Biophys. J.* 72:2002–2013.

40. Lopez, C. F., S. O. Nielsen, …, P. B. Moore. 2004. Hydrogen bonding structure and dynamics of water at the dimyristoylphosphatidylcholine lipid bilayer surface from a molecular dynamics simulation. *J. Phys. Chem. B.* 108:6603–6610.

41. Hartkamp, R., and B. Coasne. 2014. Structure and transport of aqueous electrolytes: from simple halides to radionuclide ions. *J. Chem. Phys.* 141:124508.

42. Stępniewski, M., A. Bunker, …, T. Róg. 2010. Effects of the lipid bilayer phase state on the water membrane interface. *J. Phys. Chem. B.* 114:11784–11792.

43. Leekumjorn, S., and A. K. Sum. 2006. Molecular simulation study of structural and dynamic properties of mixed DPPC/DPPE bilayers. *Biophys. J.* 90:3951–3965.

44. Róg, T., K. Murzyn, …, M. Pasenkiewicz-Gierula. 2009. Water isotope effect on the phosphatidylcholine bilayer properties: a molecular dynamics simulation study. *J. Phys. Chem. B.* 113:2378–2387.

45. Falck, E., M. Patra, …, I. Vattulainen. 2004. Lessons of slicing membranes: interplay of packing, free area, and lateral diffusion in phospholipid/cholesterol bilayers. *Biophys. J.* 87:1076–1091.

46. Marrink, S.-J., and H. J. C. Berendsen. 1994. Simulation of water transport through a lipid membrane. *J. Phys. Chem.* 98:4155–4168.

47. Norlén, L. 2001. Skin barrier structure and function: the single gel phase model. *J. Invest. Dermatol.* 117:830–836.